Effect of periodate oxidation and borohydride reduction on the chemical structure and chain conformation of arabinoxylan

Carbohydrate Polymers 376 (2026) 124811

Contents lists available at ScienceDirect

Carbohydrate Polymers

journal homepage: www.elsevier.com/locate/carbpol

Effect of periodate oxidation and borohydride reduction on the chemical structure and chain conformation of arabinoxylan

Ratchawit Janewithayapun [a,b], Hampus Karlsson [a,b,c,d], Fátima Herranz-Trillo [e], Ann E. Terry [e], Lars Evenäs [a,b,c], Fabrice Cousin [f], Anna Ström [a,b,*]

[a] Department of Chemistry and Chemical Engineering, Chalmers University of Technology, Gothenburg, SE-412 96, Sweden
[b] FibRe Centre for Lignocellulose-based Thermoplastics, Chalmers University of Technology, Gothenburg, SE-412 96, Sweden
[c] Wallenberg Wood Science Center, Chalmers University of Technology, Gothenburg, SE-412 96, Sweden
[d] Dipartimento di Chimica, Universitá degliStudi di Milano, Milano, 20122, Italy
[e] MAX IV Laboratory, Lund University, Lund, SE-221 00, Sweden
[f] Laboratoire Léon Brillouin, Université Paris-Saclay, UMR 12, CEA-CNRS, Gif Sur Yvette, 91191, France

ARTICLE INFO

Dataset link: https://doi.org/10.5281/zenodo.17726096

Keywords:
Wheat bran
Linkage analysis
Polysaccharide conformation
Small-angle X-ray scattering
NMR

ABSTRACT

The effect of periodate oxidation and borohydride reduction on arabinoxylan (AX) in aqueous solution was investigated using ^{13}C NMR spectroscopy and small-angle X-ray scattering (SAXS). AX consists of a xylose backbone, which is mono- or di-substituted with arabinose. We show that at a ring-opening modification degree of 21%, periodate oxidation occurs predominantly on arabinose, and shows a preference for arabinose linked to di-substituted xylose units over the mono-substituted. With a higher degree of modification of 33%, arabinose at the mono-substituted position and unsubstituted xylose units are also modified. At 33% a large portion of oxidizable AX residues have been ring-opened, yet SAXS reveals no significant changes in chain conformation and only a minor reduction (10%) in persistence length for the oxidized-reduced dialcohol AX. With increasing degree of oxidation, dialdehyde AX instead show an increasing tendency for aggregation, attributed to chain cross-linking. Upon reduction of the dialdehyde and cross-linked groups to dialcohol AX, the chains revert back to having repulsive interactions, acting as chains in a good solvent environment.

1. Introduction

Periodate oxidation of polysaccharides has gained popularity as a modification route for altering the macromolecular properties of polysaccharides. The reaction's selectivity for viccinal diols in polysaccharides allows for selective cleaving of carbon–carbon bonds, such as the C2-C3 bond in cellulose, resulting in a ring-opened unit with a dialdehyde functional group (Jackson & Hudson, 1937). The dialdehyde functionalities can be reduced with sodium borohydride into more chemically stable dialcohol groups (Börjesson et al., 2019; Larsson et al., 2014; Painter, 1988; Potthast et al., 2009), or further derivatized via other routes (Chemin et al., 2015; Esen & Meier, 2020; Simon et al., 2023). Through ring-opening of the rigid carbohydrate rings, it is expected that flexible hinges can be introduced to polysaccharide chains. Indeed, measurements by size-exclusion chromatography (SEC) have shown increased flexibility in oxidized and reduced (dialcohol) cellulose (Potthast et al., 2009), chitosan (Christensen et al., 2008) and alginate (Vold et al., 2006). Dialcohol cellulose in particular, has been investigated for material applications due to their improved ductility (Larsson et al., 2014; Morooka et al., 1989), lowered glass transition temperature (Simon et al., 2024) and processability by extrusion (Pellegrino et al., 2025).

Cellulose and alginate are structurally linear polysaccharides (Kristiansen et al., 2010; Vold et al., 2006), and the oxidation–reduction directly affects the polysaccharide backbone. Many polysaccharides are not structurally linear, in which case, there can be competition between ring-opening of the side groups and of the backbone (Börjesson et al., 2018; Janewithayapun et al., 2024; Kochumalayil et al., 2013). As a result, the changes in material properties can be more complex. For example, in oxidized-reduced xyloglucan, Kochumalayil et al. (2013), showed that the backbone was only modified at longer reaction times, which also corresponded with a stronger increase in film ductility measured by tensile testing.

Arabinoxylan (AX), which is of primary interest in this work, is a branched polysaccharide with a backbone of β-(1→4)-D-xylopyranosyl units, partially substituted by α-*L*-arabinofuranosyl units on *O*-3 and/or *O*-2 of the xylose units (Schooneveld-Bergmans et al., 1999). AX is

* Corresponding author at: Department of Chemistry and Chemical Engineering, Chalmers University of Technology, Gothenburg, SE-412 96, Sweden.
E-mail address: anna.strom@chalmers.se (A. Ström).

https://doi.org/10.1016/j.carbpol.2025.124811
Received 16 September 2025; Received in revised form 4 December 2025; Accepted 9 December 2025
Available online 15 December 2025

a major hemicellulose component in cereals such as wheat, rye and barley (Ebringerová et al., 2005), and can be obtained from agricultural side-streams such as wheat bran (Prückler et al., 2014). The AX content in wheat bran is similar to, or greater than the cellulose content (by weight) (Apprich et al., 2014). A better understanding of how chemical modification proceeds in branched polysaccharides can therefore benefit the development of new polysaccharide derived materials from cereal based agricultural side-streams.

The periodate oxidation of AX has been studied by Börjesson et al. (2018), with unclear conclusions on the changes in chain flexibility measured by SEC with multi-angle light scattering (SEC-MALS). Yet, dialcohol AX when further derivatized with butyl glycidyl ether (BGE), becomes three to five times more ductile than AX modified only by BGE without prior oxidation–reduction steps (Börjesson et al., 2019). Moreover, highly branched AX exhibit greater ductility after modification by the oxidation–reduction-etherification sequence, despite the AX backbone being more shielded by arabinose side groups (Janewithayapun et al., 2024). The complex and contradictory behavior raises questions on the role of the ring-opening on the properties of the thermoplastic BGE-dialcohol AX materials.

In this work, we investigate the two following hypotheses: first, that in a branched AX, oxidation–reduction modification will occur to a larger extent on the branching arabinose groups. Second, that oxidation–reduction would have an impact on the chain conformation of AX, resulting in a reduction of the chain persistence length (L_p). To answer these questions, we characterize the chemical structure of these materials in detail, in combination with small-angle X-ray scattering (SAXS) experiments for analysis of the chain conformation. We have chosen a highly substituted AX material as the model for this study, previously studied in Janewithayapun et al. (2025). This AX fraction is highly water soluble and behaves as semi-flexible chains in good solvent conditions when dispersed in water, with minor fraction of large aggregates. In comparison, lower substituted AX fractions exhibit poorer solvent interactions and contain a larger fraction of aggregates. Both time-resolved SAXS and concentration series SAXS are performed, the former providing a picture of the kinetics of structural changes during periodate oxidation, and the latter allowing for full characterization of the form factor and structure factor of ring-opened AX. The findings obtained here expand the current understanding of oxidation of branched polysaccharides through the use of AX as a model.

2. Experimental

2.1. Materials

Sodium metaperiodate ($NaIO_4$), sodium borohydride ($NaBH_4$), sodium phosphate monobasic (NaH_2PO_4) were purchased from Sigma-Aldrich (Schnelldorf, Germany). The chemicals were used without further purification. Deionized water was used throughout the experiments. Regenerated cellulose dialysis membrane (Spectra/Por 3) with a molecular weight cutoff of 3.5 kDa was purchased from Spectrum Laboratories (California, United States). AX was obtained from alkali extraction, followed by ethanol fractionation as previously reported (Janewithayapun et al., 2024). The monosaccharide composition, glycosidic linkage and weight average molar mass (M_w) of the AX used has been presented in Janewithayapun et al. (2025) (Table 1).

Table 1
Monosaccharide composition from H_2SO_4 and TFA hydrolysis, glycosidic linkages, and molar mass from SEC-MALS of the AX material used. Adapted from Janewithayapun et al. (2025) under the CC-BY license. *Abbreviations: Acid soluble lignin (ASL), galacturonic acid (GalA), glucuronic acid (GlcA).*

Monosaccharide composition			Glycosidic linkages	
Component (wt%)	H_2SO_4	TFA	Linkage pattern	mol%
			t-Ara*f*	20.6
Arabinose	42	43	2-Ara*f*	5.2
Rhamnose	n.d.	n.d.	3-Ara*f*	7.6
Galactose	4	4	5-Ara*f*	1.3
Glucose	n.d.	1	3,5-Ara*f*	n.d.
Xylose	46	50	2,5-Ara*f*	9.2
Mannose	n.d.	n.d.	Total Ara	43.8
			t-Xyl*p*	11.0
Insolubles	5	–	2-Xyl*p*	2.2
ASL	4	–	4-Xyl*p*	16.3
GalA	–	1	2,4-Xyl*p*	3.2
GlcA	–	1	3,4-Xyl*p*	10.5
			2,3,4-Xyl*p*	7.7
A/X ratio	0.90	0.86	Total Xyl	50.9
Weight average molar mass (M_w)			220 $kg \cdot mol^{-1}$	

2.2. Sample preparation for X-ray scattering experiments

2.2.1. In-situ periodate oxidation of AX

Periodate oxidation was performed as described in Janewithayapun et al. (2024) with minor modifications. 200 mL of AX solution in water at a concentration of 20 mg mL^{-1} (30.28 mmol AX) was heated at 70 °C for 3 h until dissolution was achieved, then left stirring overnight at room temperature. Isopropanol, normally added as a radical scavenger (Painter, 1988), was not used in this sample preparation to simplify the setup for continuous flow and background subtraction considerations. Periodate has been shown to be rather stable over 2 h to 3 h when kept away from daylight (Scott & Thomas, 1976), which is a similar duration to our in-situ experiment. The reaction was performed in a 250 mL Duran flask with a magnetic stirrer. To initiate the reaction, $NaIO_4$ (3.24 g, 15.14 mmol, 0.5 mol equiv.) was added to the reaction. The SAXS measurement was started and the AX solution was fed into the SAXS flowcell for measurements using an HPLC pump at a flow rate of 1 $mL \cdot min^{-1}$. SAXS scans were taken every 3 min.

2.2.2. Preparation of dialdehyde AX

For comparisons with the in-situ study, dialdehyde AX (DAX) were prepared with three target degrees of oxidation (DO) at 5%, 10% and 15% DO. Higher % DOs are not well dispersed in water, as observed in the in-situ study and hence were not prepared.

A stock solution of 0.3 g of AX in 12.4 mL water were heated at 70 °C for 3 h to achieve dissolution, and left stirring overnight at room temperature. The solution was split into three vials, for the three target % DOs. In each vial, isopropanol (0.75 mL) was added to act as a radical scavenger, as the reaction were to be left stirring overnight. Water was added to reach a final volume of 5 mL and concentration of 20 mg mL^{-1} AX (0.76 mmol).

The corresponding amount of $NaIO_4$ was added to each experiment to initiate the oxidation reaction: 0.05 mol equiv., 0.1 mol equiv. and 0.15 mol equiv., respectively, for 5% DO, 10% DO and 15% DO. The reaction vials were covered from light, to further decrease the decomposition of periodate (Painter, 1988), and stirred with a magnetic stirrer at room temperature for 20 h, at which point, no further changes were observed in the UV–Vis spectra.

The dialdehyde AX were analyzed as is (20 mg mL^{-1}), or diluted to concentrations of 4 mg mL^{-1}, and 1 mg mL^{-1}. SAXS measurements were made approximately 48 h after the initiation of the oxidation reaction, ensuring completion of the reaction. Aqueous solutions of the corresponding $NaIO_4$ concentrations were also measured.

2.2.3. Preparation of dialcohol AX

The oxidation procedure above was repeated for 100 mL of 20 mg mL^{-1} AX solution (15.14 mmol AX) but with higher equivalents of $NaIO_4$. The targeted DO for dialcohol AX (DiolAX) to be measured were 25% and 50% (0.25 equiv. and 0.5 equiv.), corresponding to $NaIO_4$ of 3.79 mmol and 7.57 mmol, respectively. After completion of the oxidation reaction, NaH_2PO_4 (0.15 g, 1.25 mmol, 0.08 equiv.) and $NaBH_4$ (1 g, 26.43 mmol, 1.75 equiv.) were dispersed in water (25 mL),

Table 2
Normalized integrals from solution state NMR experiments. The total integral should sum up to 5.0. Columns 6 and 7 show the degree of modification or oxidation from NMR and UV–Vis, respectively.

Sample	Spectrum regions and normalized integrals				Degree of modification (%)	Degree of oxidation (%)
	C1	C2/C3/C4	Int C5 +$C2_{mod}/C3_{mod}$	Total Integral	From C5+$C2_{mod}/C3_{mod}$ increase	UV–Vis DO
AX	1.0	2.9	1.0	4.9		
DiolAX21	1.0	2.7	1.3	5.0	16.9	21
DiolAX33	1.0	2.3	1.5	4.8	27.2	33

then added to the AX reaction mixture. The reaction mixture was stirred for 4 h at room temperature, after which the mixture was transferred to dialysis membranes and dialyzed against water for over 48 h. After dialysis, the mixture was frozen and freeze dried to obtain DiolAX. For SAXS measurements, the two DiolAX samples were redispersed in MilliQ water at concentrations of 20 mg mL^{-1}, 4 mg mL^{-1}, and 1 mg mL^{-1}.

2.3. Degree of oxidation from UV-Vis spectroscopy

The progress of the oxidation reaction was followed with ultraviolet spectroscopy (UV-Vis) (Cary 60 UV-Vis, Agilent technologies, California, United States) using the absorption band at λ = 290 nm, corresponding to the concentration of $NaIO_4$ (Maekawa et al., 1986). A linear standard curve for the periodate solution was obtained using concentrations of $NaIO_4$ between 0.1 mM to 5 mM. The DO from UV–Vis was calculated from the consumption of $NaIO_4$, by making the assumption that the consumption of 1 mol of $NaIO_4$ results in the oxidation of 1 mol of arabinose or xylose.

2.4. NMR spectroscopy

AX and derivatives were dissolved in DMSO-d6 by heating at 70 °C followed by sonication for 30 min. Measurements were performed on an Oxford 800 MHz magnet, with the Bruker Avance III HD spectrometer equipped with a 5 mm TXO cryoprobe operated at 45 °C. ^{13}C spectra were recorded using the WALTZ65 inverse-gated ^{1}H decoupling method with an acquisition time of 0.812 s. A ^{13}C 90° pulse of 13.4 μs was used and experiments were acquired with between 1216 to 2048 scans. The repetition time (relaxation recycle delay) was set to 5 s, which should be larger than $5\times T_1$ (for similar polysaccharide samples, we have previously obtained a ^{13}C T_1 of ~ 0.4 s). Phasing and baseline correction was performed with Topspin 4.3.0.

2.5. Small-angle X-ray scattering

SAXS experiments were performed at the CoSAXS beamline at MAX IV laboratory, Lund, Sweden. An X-ray wavelength (λ) of 1.0 Å was used and detection was done simultaneously on the SAXS detector Eiger2 4M (Dectris AG, Switzerland) and the wide-angle X-ray scattering (WAXS) detector Pilatus3 2M (Dectris AG, Switzerland). For the time-resolved experiment, detectors were positioned at distances of 2.16 m (SAXS) and 0.57 m (WAXS), covering a q range from 0.0052 $Å^{-1}$ to 0.94 $Å^{-1}$. For the isolated samples, detector distances were 10.12 m (SAXS) and 0.57 m (WAXS), covering a q range from 0.0013 $Å^{-1}$ to 0.94 $Å^{-1}$. Data reduction was carried out using the Python implementation of MatFRAIA (Jensen et al., 2022) for radial integration. The integrated data were then corrected by the dark contribution, normalized to the X-ray beam transmittance and scaled to water absolute intensity.

For the in-situ experiment, the reaction mixture was fed into the flow capillary system using an HPLC pump (Agilent 1260 Infinity II, Agilent Technologies, California, United States) as described above. Background subtraction of the processed data was carried out by scaling the water amorphous peak of the solvent (data at time (t) = 0) to the water amorphous peak at around 0.94 $Å^{-1}$ of the reaction mixture at each scan interval. The scaled background was multiplied by the solvent volume fraction and subtracted from the sample data.

For the isolated samples, samples were injected into the flow capillary system with a BioSAXS autoloader. $NaIO_4$ solutions of the corresponding concentration were measured for the background of the DAX samples, while MilliQ water was measured for the background of the DiolAX samples. The scattering of the flow capillary was subtracted from each solvent background and sample data, after which subtraction was again performed by scaling of the solvent water peak, and subtracting the solvent background multiplied by the solvent volume fraction from the sample data.

Using the approach described in Janewithayapun et al. (2025), AX scattering data was fitted to a flexible cylinder model (Pedersen & Schurtenberger, 2004), extended to include aggregate contributions at low q with a power law term (scale factor A and exponent n) and molecular scattering from monosaccharide units at high q with a Gaussian chain function (Debye, 1947) (scale factor B and radius of gyration $R_{g,\,mol}$), shown in Eq. (1). $P_{sc}(q)$ is the single chain form factor and $S_{sx}(q)$ is the cross-section scattering function. To describe the interaction effects between chains, the polymer reference interaction site model (PRISM) model was added as a structure factor, with a scale factor β and a screening correlation function with a rod form factor $c(q)$. Lastly, bkg is the q-independent background. A more detailed explanation of the model can be found in Pedersen and Schurtenberger (2004) and Janewithayapun et al. (2025).

$$I_{PRISM}(q) = \frac{I_0 P_{sc}(q) S_{xs}(q)}{1+\beta c(q) P_{sc}(q)}\left(1 + A\left(\frac{0.01}{q}\right)^n\right) + \frac{I_0}{B}\left(\frac{2\left[\exp(-Z)+Z-1\right]}{Z^2} - P_{sc}(q)S_{xs}(q)\right) + bkg \quad (1)$$

$$Z = (qR_{g,\,mol})^2 \quad (2)$$

Fitting was performed using the WLSQSAXS program (Oliveira JCP and Pedersen JS, unpublished) (Pedersen, 1997), from which it is possible to extract the chain parameters: contour length, Kuhn length and cross-section radius. From the structure factor term of the model, we extract β, which is related to the second virial coefficient (A_2) by $\beta = 2MA_2c$, where M is the molar mass and c is the concentration (Pedersen & Schurtenberger, 2004). Under dilute conditions, the value of β is taken as 0, and only the form factor is described by the model.

3. Results and discussion

3.1. Reactivity of oxidation–reduction on different AX motifs

The DO of DiolAX samples was calculated from $NaIO_4$ consumption measured by UV-Vis. This gives the mol percentage of arabinose and xylose that is expected to have reacted with $NaIO_4$ and become oxidized (Table 2). The DO of the DiolAX reacted with 0.25 equiv. $NaIO_4$ was 21%, and the DO of the DiolAX with 0.5 equiv. $NaIO_4$ was 33%. These samples are named DiolAX21 and DiolAX33, respectively. It is interesting to note that as periodate oxidation reacts on a viccinal diol group, only unsubstituted arabinose (Ara*f*) or xylose (Xyl*p*) monosaccharide residues can be oxidized. These include t-Ara*f*, t-Xyl*p* and 4-Xyl*p*, accounting for a theoretical maximum DO of 48 mol%, based on glycosidic linkage analysis (Table 1). The chemical structure of AX,

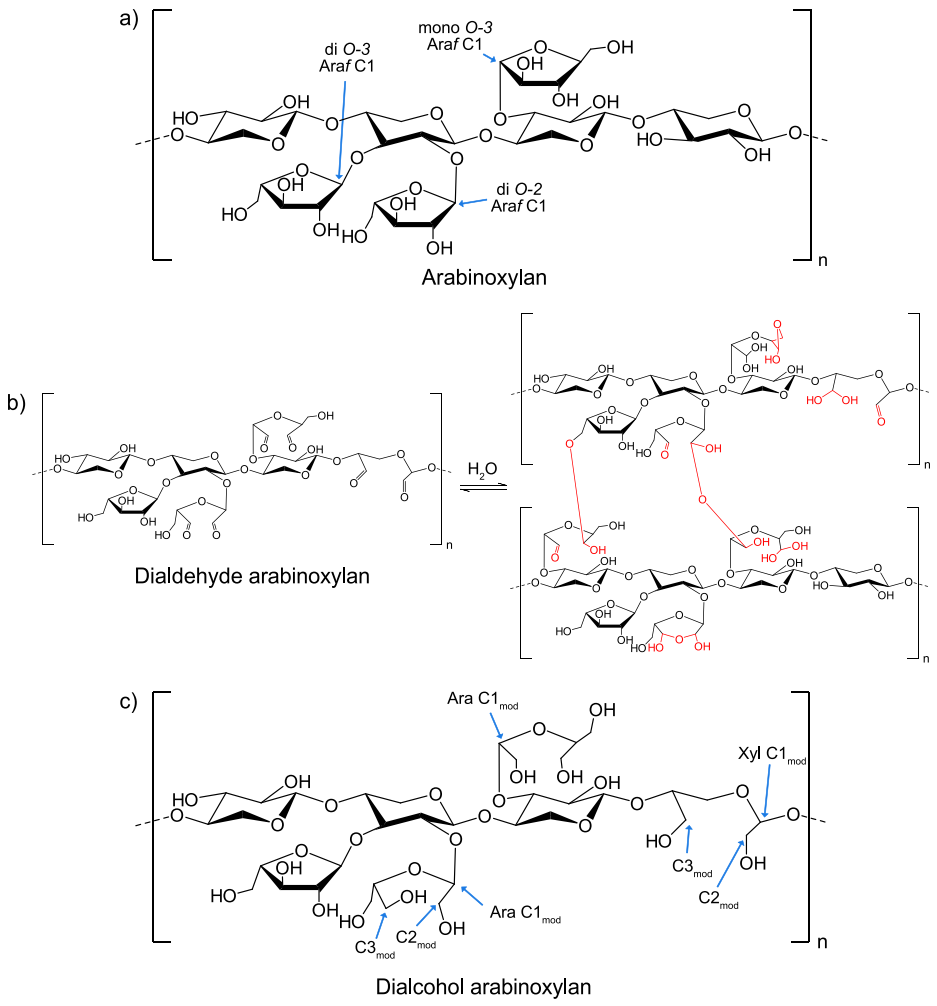

Fig. 1. Schematic representation of the chemical structure of (a) AX, (b) DAX and (c) DiolAX. The position of select peaks in ^{13}C NMR on the molecule are indicated by blue arrows. The dialdehyde functionality in DAX may further react to form intra- or inter-molecular bonds, some of the possible structures are shown in red, modified from work by Münster et al. (2017), Palasingh et al. (2021).

which is oxidized to DAX is shown in Fig. 1(a)–(b). The dialdehyde groups in DAX are not stable, and can further react in the presence of water to form hydrated aldehyde, and intra-chain or inter-chain hemialdal and hemiacetal functionalities (Amer et al., 2016; Münster et al., 2017; Palasingh et al., 2021).

After reduction with sodium borohydride, the DiolAX samples, with chemical structure shown in Fig. 1(c), could be solubilized in DMSO-d6, allowing the chemical structure to be characterized by solution state ^{13}C NMR and compared with the structure of unmodified AX. The location of some selected NMR signals on the AX/DiolAX chemical structure are also indicated in Fig. 1. In the ^{13}C NMR spectra, the Xyl*p* C1 region and the Ara*f* C1 region can be assigned as shown in Fig. 2. The Ara*f* C1 region contains three sharper signals: at 107.7 ppm, 108.4 ppm and 109.4 ppm. Assignments of these signals are based on work by Man et al. (2022), Yao et al. (2021) and from our NMR and linkage analysis measurements of low, medium and high arabinose content AX (Janewithayapun et al., 2025). The 107.7 ppm signal is assigned to mono-substituted *O*-3 Ara*f* C1, 108.4 ppm to di-substituted *O*-3 Ara*f* C1, and 109.4 ppm to a di-substituted *O*-2 Ara*f* C1. The main Xyl*p* C1 signal is centered at 102.0 ppm, with another broad signal at 99.8 ppm. The latter is assigned to the Xyl*p* C1 of a di-substituted Xyl*p* unit (2,3,4-Xyl*p*) (Yao et al., 2021).

In the ^{13}C spectra of DiolAX21, there is a significant decrease in intensity of the di-substituted *O*-2 Ara*f* C1 signal (109.4 ppm), along with a smaller decrease in intensity of the di-substituted *O*-3 Ara*f* C1 (108.4 ppm) signal. The mono-substituted *O*-3 Ara*f* C1 (107.7 ppm) and the Xyl*p* C1 (102.0 ppm) signals remains unaffected. Hence, it appears that the periodate oxidation occurs more on di-substituted Ara*f* groups. In addition to decreases in these signal intensities, a new signal develops at 104.0 ppm, which we assign to ring-opened Ara*f* C1 units (Ara C1$_{mod}$).

With increasing DO to DiolAX33, the intensity of the Ara*f* C1 signals decrease even further (Fig. 2). No sharp signals are observable in the 105 ppm to 110 ppm range. The evolution of the C1 region of the spectra across both DiolAX samples show that Ara*f* groups are oxidized most preferrably on the di-substituted *O*-2 Ara*f* units, followed by di-substituted *O*-3 Ara*f*, and lastly the mono-substituted *O*-3 Ara*f*. As essentially only the unsubstituted terminal Ara*f* can be oxidized by $NaIO_4$ (20.6 mol% from Table 1), any Ara*f* units that can be oxidized are likely already ring-opened at this DO, and we assign the residual broad signals in this region to non-terminal Ara*f* residues (e.g. 2-Ara*f* or 2,5-Ara*f*), as these residues would lack the vicinal diol groups required for periodate oxidation. For DiolAX33, there is also a small decrease in the Xyl*p* C1 signal at 102.0 ppm, and a new signal at 103.0 ppm, assigned to ring-opened Xyl*p* C1 (Xyl C1$_{mod}$), based on the ^{13}C spectrum of ring-opened beechwood xylan (Palasingh et al., 2022). The changes in the Xyl*p* signals, therefore indicate oxidation of Xyl*p* units as well at higher DO. The prevalence of oxidation on the di-substituted Ara*f* could be explained as a result of substituted regions of the AX chain having more extended conformations, and therefore, more accessible by the periodate salt.

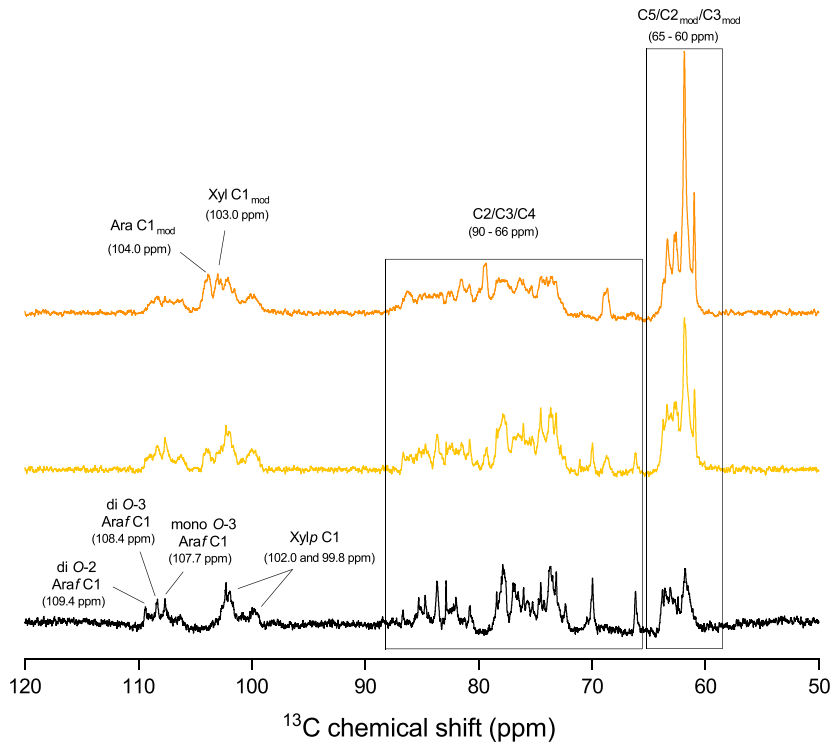

Fig. 2. ^{13}C NMR spectra (from top to bottom) of DiolAX33 (orange), DiolAX21 (yellow) and AX (black) in DMSO-d6.

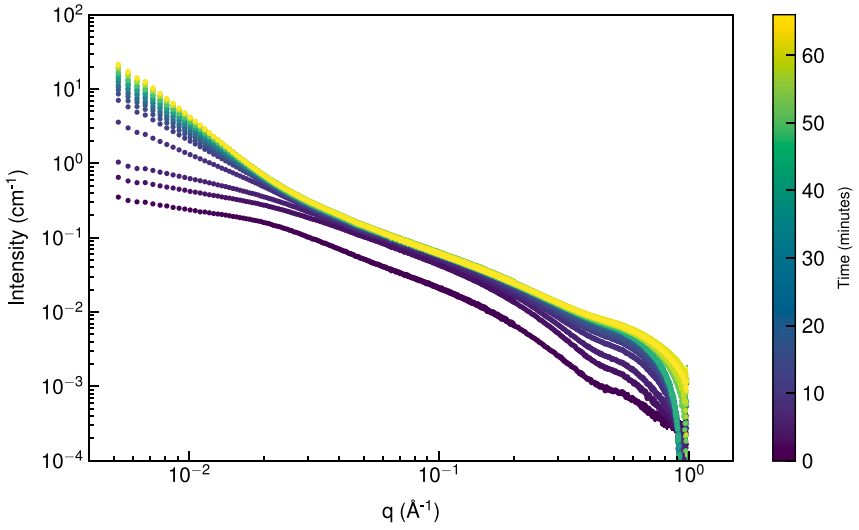

Fig. 3. In-situ time-resolved SAXS data of AX-water dispersion at a concentration of 20 mg mL^{-1} during oxidation with 0.5 equiv. of $NaIO_4$. SAXS scans were obtained from reaction time $t = 0$ min to $t = 66$ min at 3 min intervals.

In other regions of the spectras, a decrease in the C2/C3/C4 region is observed simultaneously with an increase in the intensity of the C5 region (65 – 60 ppm) due to an upfield shift of modified $C2_{mod}/C3_{mod}$ signals (Karlsson et al., 2024). The C2/C3/C4 regions have been grouped by comparison with assignments by Brillouet and Joseleau (1987), Man et al. (2022), Elschner et al. (2023). 2D correlation spectroscopy have also been conducted to help assignments. The ^1H spectra show similar changes in the H1 region (4.0 – 5.5 ppm), as observed in the C1 region but the ^1H signals were more overlapped (Figure S1, supplementary information). All NMR datasets are available, see section on Data Availability.

Following the approach of Karlsson et al. (2024), the degree of modification of DiolAX can be estimated using the increase in the integral of the $C5/C2_{mod}/C3_{mod}$ peaks relative to the $C1/C1_{mod}$ peaks, which is complementary to the DO from UV-Vis. The results are shown in Table 2, and are in agreement with the DO obtained from UV–Vis, with slightly lower values from the NMR method. The main contributor to the uncertainties in the degree of modification obtained in fact comes from obtaining a good baseline correction of the solution ^{13}C spectra from the high field spectrometer.

Comparisons between NMR, UV-Vis (and other) methods for determining the degree of ring-opening has also been investigated in oxidized xylan (Palasingh et al., 2022), cellulose nanocrystal (CNC) (Llàcer Navarro et al., 2021), cellulose fiber (Karlsson et al., 2024) and microcrystalline cellulose systems (MCC) (Karlsson et al., 2024). The overall conclusion has been that the UV-Vis method, which measures DO at the oxidation step, tends to produce higher values than NMR measurement of the degree of modification at the oxidized-reduced

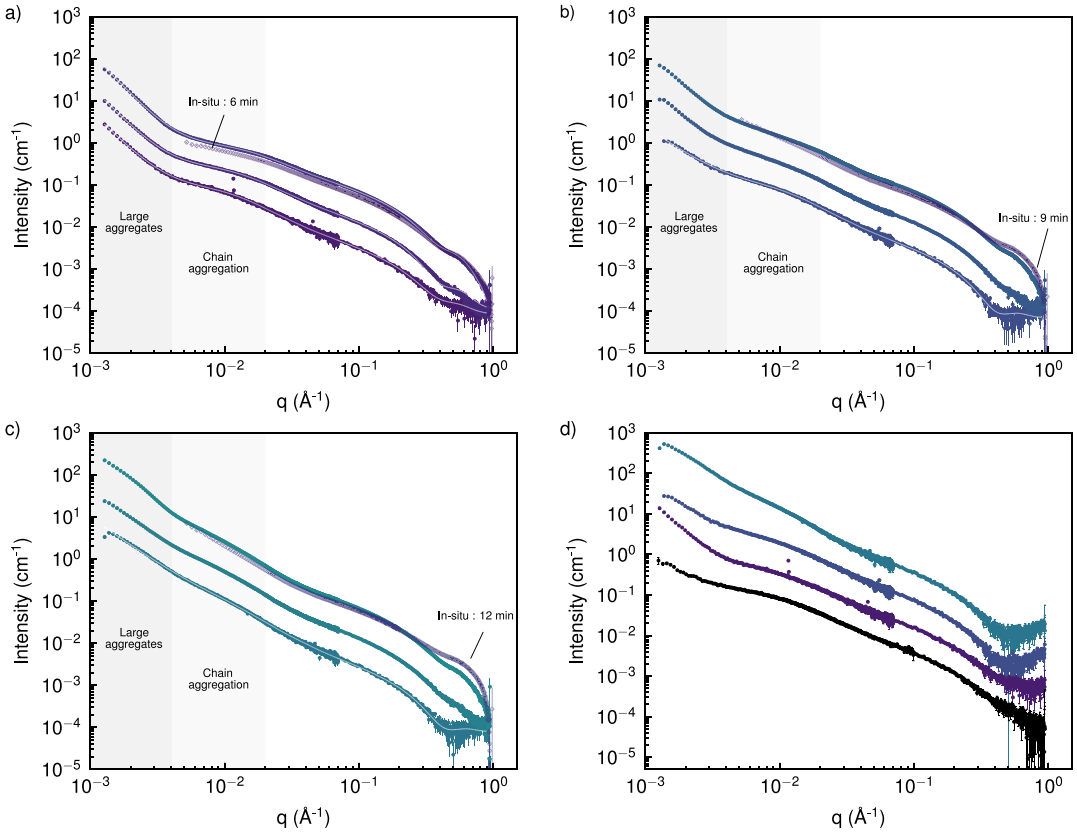

Fig. 4. SAXS data of (a) DAX5, (b) DAX10, and (c) DAX15 at concentrations of 1 mg mL^{-1}, 4 mg mL^{-1} and 20 mg mL^{-1}. Data from the in-situ experiment at different time points (6 min, 9 min and 12 min) are shown as open symbols. Lines show fitting to the flexible cylinder model in Eq. (1), note that higher concentrations of DAX10 and DAX15 are not described by the model. (d) Comparisons of SAXS data of AX, DAX5, DAX10 and DAX15 at 1 mg mL^{-1}. DAX5 data is shifted by a factor of 5, DAX10 by 25, and DAX15 by 125 for ease of viewing.

dialcohol step (Karlsson et al., 2024; Palasingh et al., 2022). However, the extent of overestimation seems dependent on the substrate. In oxidized AX (this work), xylan, and CNC systems, the DO determined from the UV-Vis method is higher, but by less than 10% units. In MCC systems, the overestimation by UV-Vis was larger, at ~ 20% units. The MCC system is heterogenous on a larger length scale, where the oxidation and reduction reaction may not occur as efficiently. This could explain the larger overestimation by the UV-Vis method, which is based on $NaIO_4$ consumption being equivalent to the oxidation of a viccinal diol group and does not assess the following reduction step of the aldehyde groups to dialcohol groups.

3.2. In-situ oxidation with time-resolved SAXS

Data from the in-situ experiment are shown in Fig. 3. The AX concentration was chosen to be the same as in the actual synthesis (20 mg mL^{-1}). This concentration is higher than the critical overlap concentration c* of 8 mg mL^{-1} (Janewithayapun et al., 2025), where the dispersion goes from the dilute to semi-dilute regime. Therefore, both the intra-chain form factor and the inter-chain structure factor are probed in this in-situ SAXS experiment. The HPLC pump setup induces a delay between the reaction's initiation in the reaction vessel and its transport to the X-ray beam's flowcell. The first detection of the reaction mixture at the flowcell occurs 15 min after the initiation of the reaction and this point is assigned as $t = 0$ min of the reaction. A lowered intensity is also observed at $t = 0$ min, due to residual water in the tubing diluting the AX dispersion initially.

The strongest change in the scattering features occurs in the low q region $0.005 < q < 0.02$ Å^{-1}. From the start of the oxidation reaction at $t = 0$ min, an increase in the steepness and intensity of the low q region is observed already at $t = 6$ min. Between $t = 6$ min and $t = 9$ min, the largest change in steepness and intensity at low q occurs, after which the increase of steepness and intensity becomes more gradual. The scattering intensity at low q values is associated with fluctuations of scattering length density at large length-scales. In dilute solutions or suspensions of non-interacting objects, the low q region enables the determination of the R_g of objects if the experimental q-range covers this lengthscale. This is observed as a leveling-off of the intensity at low q values, forming a Guinier plateau. When structures are larger than the q-range probed, no such plateau is observed. Given the lowest q measured in the in-situ SAXS setup is 0.007 Å^{-1}, the lack of any observable Guinier plateau means that structures larger than 14 nm (estimated from $qR_g < 1$) are formed with increasing reaction time of oxidation. Inter-molecular bonds can be formed from oxidized di-aldehyde groups (Münster et al., 2017; Palasingh et al., 2021; Veelaert et al., 1997); as such, the rate of the increasing contribution of the low q component to the scattering intensity is reflective of the rate of the inter-molecular reactions during the oxidation of AX, resulting in aggregation of individual chains.

In the intermediate q region between $0.02 < q < 0.1$ Å^{-1}, the scattering intensity is sensitive to changes in the chain conformation statistics i.e. in their Flory exponent (ν) or mass fractal, as well as the L_p. At the concentration used in this in-situ experiment (~ 20 mg mL^{-1}), these two features are affected by concentration effects, however, large variations in behavior should still be qualitatively observable. For instance, a decrease in L_p from 15 nm to 5 nm as in alginate (Vold et al., 2006), or a transition from stiff extended chains to partially collapsed chains, as in cellulose (Potthast et al., 2007), should produce significantly different features in the SAXS data of the AX. In our case, the absence of changes in the intermediate q region of the in-situ

data demonstrates that almost no change in chain compactness or L_p occurred during this oxidation of AX (0.5 equiv. $NaIO_4$). Note again that 0.5 equiv. $NaIO_4$ should be close to the maximum obtainable DO based on unsubstituted Ara*f* and Xyl*p* units.

Lastly, the high q ($q > 0.2$ Å^{-1}) features of the scattering intensity probes the scattering of the cross-section of the AX chain, as well as molecular scattering from Ara*f* and Xyl*p* units. In this q range, the largest change is an increase in the q-independent background level with reaction time. This could be related to a change of the scattering intensity of the solvent due to variations in the concentration of $NaIO_4$ in the tubing.

3.3. The conformation of DAX

The time-resolved measurements allow a comparison of separately prepared DAX at known DOs with in-situ data at different time points. DAX with UV–Vis determined DO of 5%, 10% and 15% are separately measured, so that the form factor of DAX could be studied in more detail in both semi-dilute and dilute conditions (Fig. 4). These samples are named DAX5, DAX10, and DAX15, respectively, after their UV–Vis DO.

The scattering data of DAX5 closely resembles that of the time-resolved data at $t = 6$ min, of DAX10 at $t = 9$ min, and of DAX15 at $t = 12$ min. Comparisons between in-situ and isolated sample data are shown in Fig. 4(a)–(c). It is interesting therefore, to note that the structural changes occur already at low DOs. By separately studying the conformation of these DAX at different concentrations, a clearer picture of the effect of periodate oxidation on the form factor is obtained. Note that the SAXS data for these concentration series were obtained at a longer sample-detector distance, and goes to lower q values than for the in-situ SAXS experiment.

From high to low q, the scattering features of AX include: the cross-section contribution, followed by a transition at $\sim q = 0.2$ Å^{-1} to a q^{-1} scaling stemming from rigid, rod-like chain segments. At intermediate q ($\sim q = 0.05$ Å^{-1}), the chain's conformation statistic is probed, where the q scaling follows the inverse of ν as $q^{-1/\nu}$. Lastly, at low q ($\sim q = 0.01$ Å^{-1}), a Guinier plateau begins to form as real space distances larger than the chain length are probed, however, the leveling-off is overlapped with the upturn from larger aggregates at lowest q. In DAX10 and DAX15, an upturn at low q is observed where the Guinier plateau starts to be visible in AX and DAX5 (between $0.004 < q < 0.02$ Å^{-1}). The upturn occurs in the same q range as in the in-situ experiment, and is associated to the aggregation of the chains due to cross-linking reactions. This chain aggregation is separate from contributions by larger aggregates at the lowest q values ($q < 0.004$ Å^{-1}). The two different regions are also indicated in Fig. 4.

From the concentration series, the inter-chain structure factor related to polymer interactions can be determined. Janewithayapun et al. (2025) showed that this fraction of branched AX exhibits scaling behavior of chains in a good solvent, with a decrease in the scattering intensity for the chains at low q when normalized against concentration. The scaling behavior is related to the second virial coefficient A_2 of the polymer (Pedersen & Schurtenberger, 2004), which is positive for a polymer in a good solvent environment, representing repulsive interaction pair potential. In systems with attractive interactions, such as in those with tendencies for aggregation, A_2 takes on negative values (Bonneté et al., 1999; Lindner, 2002). The same type of concentration normalized SAXS intensity plots were made for DAX samples, shown in Figure S2 of the supplementary information. From the plots, we observe that DAX5 shows a decrease in low–intermediate q intensity (0.005 to 0.02 Å^{-1}) at higher concentrations. Furthermore, the intensity at the lowest q values do not increase, showing that no concentration dependent aggregation is occurring. DAX5 still behaves therefore, as chains in a good solvent with repulsive interactions. For DAX10 and DAX15, we see that the normalized intensity at low-intermediate q is unchanged with concentration, and the intensity at lowest q instead increases. These behaviors indicate aggregating tendencies, and thus negative A_2 for the two samples with higher oxidation degree.

To analyze the form factor, we perform fitting of the 1 mg mL^{-1} concentration samples, which is below the c^* of AX of 8 mg mL^{-1} (Janewithayapun et al., 2025). We have previously shown that the scattering intensity of highly branched AX can be represented by the flexible cylinder model with positive excluded volume effects (good solvent conditions) as shown in Eq. (1). The same model is selected, therefore, to analyze changes in the conformation that may occur after oxidation.

The flexible cylinder model describes well the scattering intensity of all three DAX samples, showing that the DAX chains still exhibit positive excluded volume at length scales smaller than the chain aggregation. At high q (> 0.75 Å^{-1}), solvent subtraction becomes difficult (Fig. 4(a)–(c)), therefore, these data points were excluded from the fitting. For the same reason, the parameters B and $R_{g,mol}$ describing the scattering contribution of monosaccharide units at high q are difficult to determine and the associated standard errors are large. The fitted parameters from the flexible cylinder model are shown in Table 3. Of highest interest is the evolution of L_p (Kuhn length = 2 L_p) with DO, where the fitted L_p for DAX5 was 4.6 nm, very close to the value of unmodified AX. Two other parameters of interest are the contour length and the $I(0)$ which is the scattering intensity at $q = 0$, the two are related to the z-average molar mass and the weight average molar mass of the chains, respectively (Pedersen & Schurtenberger, 2004; Plazzotta et al., 2016). The contour length from fitting was 95 nm and $I(0)$ was 0.10 cm^{-1}. Both of these parameters are similar to, or larger than, values obtained for AX, indicating no observable decrease in chain length or molar mass.

Similar fits were performed for DAX10 and DAX15, showing an increase in the scale factor of the power law term as a result of increased chain aggregation. The fitted L_p was 4.4 nm for the DAX10 and 3.7 nm for the DAX15. However, since aggregation has occurred to a larger extent, the fitted L_p are only apparent values of L_p. Therefore, it is important to compare these values to those fitted for reduced DiolAX with fewer aggregates, discussed in the following section. The fitted contour lengths are 101 nm and 129 nm, while the $I(0)$ are 0.11 cm^{-1} and 0.12 cm^{-1} for DAX10 and DAX15, respectively. L_p and contour lengths obtained indicate increased chain length, which is likely again a result of chain cross-linking and subsequent aggregation.

The model described in Eq. (1) with the PRISM structure factor can be used to quantitatively compare the scaling behavior of AX and DAX5, which both show repulsive interactions. As the molar mass is difficult to determine for the cross-linked samples, we choose to compare only $2MA_2$, which can be determined from the slope of a plot of the parameter β (where $\beta = 2MA_2c$) as a function of concentration (Figure S3, supplementary information). The value of β for AX has been adapted from Janewithayapun et al. (2025), where, given that interactions were small at a concentration of 1 mg mL^{-1} (minor structure factor effects), we set the value of β to 0 at 1 mg mL^{-1} to have the same concentration series as the samples in this work.

The values of the slope of β against c for each derivative is shown in Fig. 5. The slope for DAX5 is lower than that of AX, and the slope would be negative for DAX10 and DAX15. The PRISM model in Eq. (1) was not designed to describe aggregation (Pedersen & Schurtenberger, 2004) as occurs in DAX10 and DAX15, however, their attractive interactions would correspond to negative values of A_2. We therefore conclude that there is a decreasing trend of A_2 with increasing DO, transitioning from repulsive interactions, as observed for chains in good solvent conditions (AX, DAX5), to aggregating tendencies (DAX10, DAX15).

3.4. Conformation of DiolAX

Upon reduction with excess $NaBH_4$, derivatives of the dialdehyde group in DAX, including cross-links, are reduced to dialcohol groups.

Table 3
Fitted parameters of AX and isolated DAX samples at 1 mg mL^{-1} to the flexible cylinder model shown in Eq. (1). Reduced chi-squared (χ^2_R) values are 1.4, 4.1, 1.5 and 2.5, respectively, for AX, DAX5, DAX10 and DAX15. R_g is calculated from the contour length as in Pedersen and Schurtenberger (2004). "~" indicates fitted values where the associated errors are large. Data for AX reproduced from Janewithayapun et al. (2025) under the CC-BY license.

Parameter	AX	DAX5	DAX10	DAX15
$I(0)$ (cm^{-1})	0.108 ± 0.002	0.101 ± 0.002	0.109 ± 0.002	0.123 ± 0.005
Contour length (nm)	85.1 ± 2.3	94.8 ± 4.1	101.4 ± 3.0	129.2 ± 9.1
Kuhn length (nm)	9.0 ± 0.3	9.3 ± 0.6	8.8 ± 0.3	7.3 ± 0.6
R_{xs} (Å)	9.9 ± 0.3	8.9 ± 0.5	8.4 ± 0.4	7.9 ± 0.7
Background (cm^{-1})	$-2.3 \times 10^{-5} \pm 0.9 \times 10^{-5}$	$5.3 \times 10^{-5} \pm 1.9 \times 10^{-5}$	$\sim 6 \times 10^{-5} \pm 10 \times 10^{-5}$	$\sim 8 \times 10^{-5} \pm 10 \times 10^{-5}$
Scale power law	0.119 ± 0.010	0.045 ± 0.004	0.128 ± 0.008	0.50 ± 0.03
Exponent power law	1.82 ± 0.04	3.10 ± 0.04	2.23 ± 0.03	2.20 ± 0.01
B	142 ± 25	319 ± 183	$\sim 2.5 \times 10^3 \pm 2.5 \times 10^3$	$\sim 5 \times 10^3 \pm 30 \times 10^3$
$R_{g,mol}$ (Å)	5.3 ± 0.7	5 ± 2	~ 3 ± 15	~ 4 ± 41
R_g (nm)	11.2	12.1	12.4	13.4

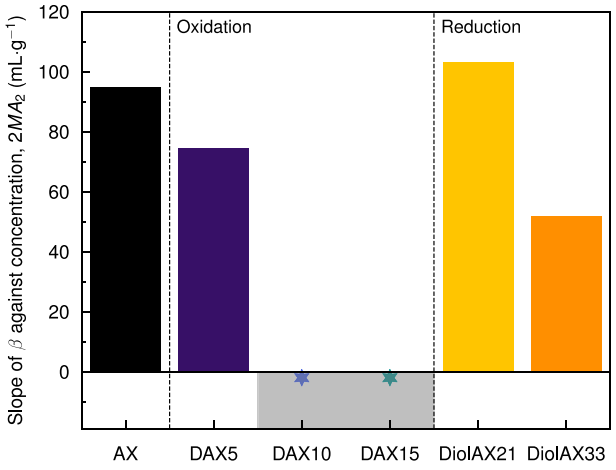

Fig. 5. Linear fitted values of the slope from the structure factor parameter β against concentration plot. *DAX10 and DAX15 were not described by the PRISM model, however, their aggregation tendencies indicate a negative value for A_2, here represented by the gray shaded region.

We therefore chose to study DiolAX at higher degree of modification than for DAX, where such high DO for DAX would result in indispersible aggregates. The SAXS data for DiolAX at 21% and 33% DO are measured at the same three concentrations as above (Fig. 6). From the scattering data, it is apparent that the low q chain aggregation features from cross-linking are not present in DiolAX samples.

The scattering features for both DiolAX21 and DiolAX33 are similar to each other, and to AX, as shown in Fig. 6(a)–(b), over almost the whole q range down to 0.008 Å^{-1}. The largest difference between the samples is the exponent and scale of the low q power law region. Utilizing the same flexible cylinder model, the fitted L_p are obtained as 4.0 nm and 3.9 nm for DiolAX21 and DiolAX33, respectively (see Table 4). The reduction in L_p is only approximately 10% between AX and DiolAX33. The two DiolAX are modified to even higher degree than DAX15, which has an apparent L_p of 3.7 nm. Therefore, the decrease in L_p for DAX10 and DAX15 can be attributed to aggregation, resulting in screening of the true L_p of the chains. This observation is interesting, as it demonstrates that measuring the L_p of a semi-flexible polymer under aggregation (DAX) can indeed result in a lower observed L_p compared to a similar polymer that is well dispersed (DiolAX).

For comparisons of $I(0)$, thus of changes in M_w, the scattering data of AX, DiolAX21 and DiolAX33 are scaled to be equal at high q (Fig. 6(a)). A small decrease in both $I(0)$ and contour length is observed in DiolAX33 compared to DiolAX21, however these values are still similar to or higher than those of unmodified AX. It is possible that the modification, followed by purification (from chemical reagents) using

Table 4
Fitted parameters of AX, DiolAX21 and DiolAX33 at 1 mg mL^{-1} to the flexible cylinder model (Eq. (1)). χ^2_R was 1.3 for both DiolAX21 and DiolAX33.

Parameter	DiolAX21	DiolAX33
I(0) (cm^{-1})	0.117 ± 0.002	0.105 ± 0.007
Contour length (nm)	95.8 ± 2.2	89.8 ± 6.0
Kuhn length (nm)	8.0 ± 0.2	7.8 ± 0.4
R_{xs} (Å)	9.0 ± 0.3	9.3 ± 0.3
Background (cm^{-1})	$-4.6 \times 10^{-5} \pm 1.9 \times 10^{-5}$	$-5.3 \times 10^{-5} \pm 1.5 \times 10^{-5}$
Scale power law	0.111 ± 0.006	0.47 ± 0.07
Exponent power law	2.51 ± 0.03	1.31 ± 0.05
B	208 ± 33	154 ± 27
$R_{g,mol}$ (Å)	4.0 ± 0.7	4.4 ± 0.7
R_g (nm)	11.5	11.0

dialysis resulted in the removal of smaller molecules. Following this reasoning, there is likely some reduction in molar mass with oxidation between DiolAX21 and DiolAX33 but we are not able to quantify this.

The same analysis of the concentration series was performed for DiolAX21 and DiolAX33. From the concentration normalized scattering intensity plots, we see that both DiolAX samples show the scaling behavior of chains in a good solvent environment (Figure S4, supplementary information). For quantitative analysis, the structure factor and its fitted parameter β are again obtained from fitting the model in Eq. (1) (Fig. 6(c)–(d)). The slope of the plot of β against concentration in Fig. 5 indicates, assuming a similar M for all three materials, that the values of A_2 are: AX ≈ DiolAX21 > DiolAX33, showing lower solvent quality in water for DiolAX33, although all materials are in good solvent environments. It should also be taken into account that the fits of β for DiolAX33 could be affected by the distinct low q aggregate contribution shape of DiolAX33 at 1 mg mL^{-1} (Fig. 6(a)). It is clear that the strong inter-molecular interactions present in DAX can be removed by reduction with $NaBH_4$. The decrease in solvent quality at the highest degree of oxidation could be a result of a lowered steric hindrance for chain interactions provided by arabinose side groups (Andrewartha et al., 1979) after ring-opening.

4. Conclusions

^{13}C NMR spectroscopy shows that periodate oxidation and reduction proceed with preferences for specific motifs in the AX chain. Ara*f* in di-substituted *O*-2 Ara*f* positions are oxidized most at a lower degree of modification, followed by di-substituted *O*-3 Ara*f*, then, by the mono-substituted *O*-3 Ara*f* and unsubstituted Xyl*p* units at a higher degree of modification.

Analysis of in-situ oxidation SAXS and concentration series SAXS data reveal that no large change in chain conformation or L_p occurs during the oxidation of AX. Instead, an increase in scattering intensity was observed at low q which is attributed to the cross-linking of DAX chains. Additionally, the second virial coefficient (A_2) obtained

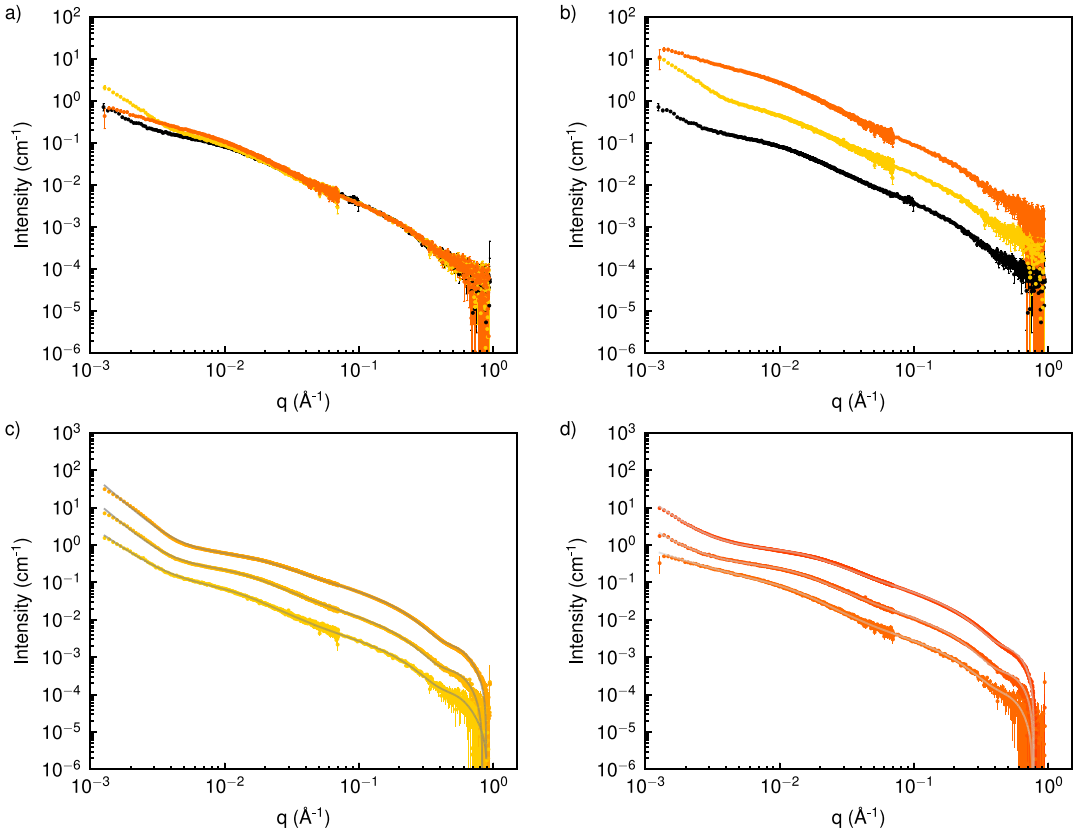

Fig. 6. SAXS data of (a) AX (black), DiolAX21 (yellow) and DiolAX33 (orange) at 1 mg mL^{-1}, and comparisons in (b) where DiolAX21 data is shifted by a factor of 5, and DiolAX33 by a factor of 25 for ease of viewing. SAXS data of (c) DiolAX21 and (d) DiolAX33 at concentrations of 1 mg mL^{-1}, 4 mg mL^{-1} and 20 mg mL^{-1}, lines show a fit to the model in Eq. (1).

from fitting of the DAX structure factor decreases with DO, further showing that inter-molecular interactions between DAX chains become attractive.

The SAXS data of reduced DiolAX show that reduction of the aldehyde groups by $NaBH_4$ removes the contributions from cross-linked chains, allowing the L_p to be more accurately determined. In DiolAX33, the reduction in L_p is approximately 10%, relative to AX, which is a smaller decrease than was observed in alginate or chitosan, where the decrease in L_p was reduced by a factor of 2 to 3 (Christensen et al., 2008; Vold et al., 2006). The A_2 of the two DiolAX are positive and they behave as chains in the good solvent regime. However, assuming similar M, the A_2 of DiolAX33 would be lower, indicating that interactions with water is less favorable for DiolAX33 as compared to AX.

We conclude that the oxidation and reduction of a branched polysaccharide, such as AX, proceeds differently than in linear polysaccharides. This is reasoned to be a result of modification occurring predominantly at the branching side groups, leading to the backbone not being altered to the same extent. Therefore, an increase in the flexibility of the chains does not occur, contrary to the case for linear polysaccharides, or is not as pronounced.

CRediT authorship contribution statement

Ratchawit Janewithayapun: Writing – original draft, Visualization, Methodology, Investigation, Formal analysis, Conceptualization. **Hampus Karlsson:** Writing – review & editing, Methodology, Investigation. **Fátima Herranz-Trillo:** Writing – review & editing, Investigation, Resources. **Ann E. Terry:** Writing – review & editing, Investigation, Resources. **Lars Evenäs:** Writing – review & editing, Methodology. **Fabrice Cousin:** Writing – review & editing, Supervision, Funding acquisition. **Anna Ström:** Writing – review & editing, Supervision, Project administration, Funding acquisition.

Funding sources

We acknowledge the financial contribution from Formas – Swedish Research Council for Sustainable Development, with grant number 2020-01235.

Declaration of competing interest

The authors declare that they have no known competing financial interests or personal relationships that could have appeared to influence the work reported in this paper.

Acknowledgments

We acknowledge the Swedish NMR centre in Gothenburg for access to NMR spectrometers and MAX IV Laboratory for time on beamline CoSAXS under Proposal 20221186 and 20231013. Research conducted at MAX IV, a Swedish national user facility, is supported by the Swedish Research council under contract 2018-07152, the Formas – Swedish Research Council for Sustainable Development is acknowledged for funding with grant number 2020-01235.

Appendix A. Supplementary information

Supplementary information available, showing ^{1}H NMR spectra and additional SAXS fitting parameters and data.

Supplementary material related to this article can be found online at https://doi.org/10.1016/j.carbpol.2025.124811.

Data availability

Datasets for NMR and SAXS can be found at https://doi.org/10.5281/zenodo.17726096.

References

Amer, H., Nypelö, T., Sulaeva, I., Bacher, M., Henniges, U., Potthast, A., & Rosenau, T. (2016). Synthesis and characterization of periodate-oxidized polysaccharides: Dialdehyde Xylan (DAX). *Biomacromolecules*, *17*(9), 2972–2980. http://dx.doi.org/10.1021/acs.biomac.6b00777.

Andrewartha, K. A., Phillips, D. R., & Stone, B. A. (1979). Solution properties of wheat-flour arabinoxylans and enzymically modified arabinoxylans. *Carbohydrate Research*, *77*(1), 191–204.

Apprich, S., Özge Tirpanalan, Hell, J., Reisinger, M., Böhmdorfer, S., Siebenhandl-Ehn, S., Novalin, S., & Kneifel, W. (2014). Wheat bran-based biorefinery 2: Valorization of products. *LWT - Food Science and Technology*, *56*(2), 222–231. http://dx.doi.org/10.1016/j.lwt.2013.12.003.

Bonneté, F., Finet, S., & Tardieu, A. (1999). Second virial coefficient: variations with lysozyme crystallization conditions. *Journal of Crystal Growth*, *196*(2), 403–414. http://dx.doi.org/10.1016/S0022-0248(98)00826-4.

Börjesson, M., Larsson, A., Westman, G., & Ström, A. (2018). Periodate oxidation of xylan-based hemicelluloses and its effect on their thermal properties. *Carbohydrate Polymers*, *202*, 280–287. http://dx.doi.org/10.1016/j.carbpol.2018.08.110.

Börjesson, M., Westman, G., Larsson, A., & Ström, A. (2019). Thermoplastic and flexible films from arabinoxylan. *ACS Applied Polymer Materials*, *1*(6), 1443–1450.

Brillouet, J. M., & Joseleau, J. P. (1987). Investigation of the structure of a heteroxylan from the outer pericarp (beeswing bran) of wheat kernel. *Carbohydrate Research*, *159*(1), 109–126. http://dx.doi.org/10.1016/S0008-6215(00)90009-0.

Chemin, M., Rakotovelo, A., Ham-Pichavant, F., Chollet, G., da Silva Perez, D., Petit-Conil, M., Cramail, H., & Grelier, S. (2015). Synthesis and characterization of functionalized 4-O-methylglucuronoxylan derivatives. *Holzforschung*, *69*(6), 713–720. http://dx.doi.org/10.1515/hf-2014-0290.

Christensen, B. E., Vold, I. M. N., & Vårum, K. M. (2008). Chain stiffness and extension of chitosans and periodate oxidised chitosans studied by size-exclusion chromatography combined with light scattering and viscosity detectors. *Carbohydrate Polymers*, *74*(3), 559–565. http://dx.doi.org/10.1016/j.carbpol.2008.04.012.

De Man, W. L., Chandran, C. V., Wouters, A. G., Radhakrishnan, S., Martens, J. A., Breynaert, E., & Delcour, J. A. (2022). Hydration of wheat flour water-unextractable cell wall material enables structural analysis of its arabinoxylan by high-resolution solid-state 13C MAS NMR spectroscopy. *Journal of Agricultural and Food Chemistry*, *70*(34), 10604–10610. http://dx.doi.org/10.1021/acs.jafc.2c04087.

Debye, P. (1947). Molecular-weight determination by light scattering. *The Journal of Physical and Colloid Chemistry*, *51*(1), 18–32. http://dx.doi.org/10.1021/j150451a002.

Ebringerová, A., Hromádková, Z., & Heinze, T. (2005). Hemicellulose. In *Polysaccharides i: structure, characterization and use* (pp. 1–67). Berlin, Heidelberg: Springer Berlin Heidelberg, http://dx.doi.org/10.1007/b136816.

Elschner, T., Brendler, E., & Fischer, S. (2023). Overcoming challenges in the synthesis of a lignin-carbohydrate complex (LCC) model: mitsunobu versus appel product. *Cellulose*, *30*(4), 2111–2121.

Esen, E., & Meier, M. A. R. (2020). Sustainable functionalization of 2,3-dialdehyde cellulose via the passerini three-component reaction. *ACS Sustainable Chemistry & Engineering*, *8*(41), 15755–15760. http://dx.doi.org/10.1021/acssuschemeng.0c06153.

Jackson, E. L., & Hudson, C. S. (1937). Application of the cleavage type of oxidation by periodic acid to starch and Cellulose1. *Journal of the American Chemical Society*, *59*(10), 2049–2050. http://dx.doi.org/10.1021/ja01289a077.

Janewithayapun, R., Cousin, F., de Moura Pereira, P. F., Herranz-Trillo, F., Terry, A. E., Pedersen, J. S., Jiménez-Quero, A., & Ström, A. (2025). Correlation between arabinose content and the conformation of arabinoxylan in water dispersions. *Carbohydrate Polymers*, *368*, Article 124082. http://dx.doi.org/10.1016/j.carbpol.2025.124082.

Janewithayapun, R., Hedenqvist, M. S., Cousin, F., Idström, A., Evenäs, L., Lopez-Sanchez, P., Westman, G., Larsson, A., & Ström, A. (2024). Nanostructures of etherified arabinoxylans and the effect of arabinose content on material properties. *Carbohydrate Polymers*, *331*, Article 121846. http://dx.doi.org/10.1016/j.carbpol.2024.121846.

Jensen, A. B., Christensen, T. E. K., Weninger, C., & Birkedal, H. (2022). Very large-scale diffraction investigations enabled by a matrix-multiplication facilitated radial and azimuthal integration algorithm: Matfraia. *Journal of Synchrotron Radiation*, *29*(6), 1420–1428.

Karlsson, H., Svenningsson, L., Storm, R., Chaiyupatham, P., Brolin, A., Larsson, A., Pinon, A. C., Schantz, S., Karlson, L., Larsson, P. A., et al. (2024). Dynamic nuclear polarization solid-state NMR spectroscopy as a tool to rapidly determine degree of modification in dialcohol cellulose. *Cellulose*, *31*(18), 10727–10744.

Kochumalayil, J. J., Zhou, Q., Kasai, W., & Berglund, L. A. (2013). Regioselective modification of a xyloglucan hemicellulose for high-performance biopolymer barrier films. *Carbohydrate Polymers*, *93*(2), 466–472. http://dx.doi.org/10.1016/j.carbpol.2012.12.041.

Kristiansen, K. A., Potthast, A., & Christensen, B. E. (2010). Periodate oxidation of polysaccharides for modification of chemical and physical properties. *Carbohydrate Research*, *345*(10), 1264–1271. http://dx.doi.org/10.1016/j.carres.2010.02.011.

Larsson, P. A., Berglund, L. A., & Wågberg, L. (2014). Ductile all-cellulose nanocomposite films fabricated from core–shell structured cellulose nanofibrils. *Biomacromolecules*, *15*(6), 2218–2223. http://dx.doi.org/10.1021/bm500360c.

Lindner, P. (2002). Chapter 2 - scattering experiments: Experimental aspects, initial data reduction and absolute calibration. In *Neutrons, x-rays and light: scattering methods applied to soft condensed matter* (pp. 23–48). Elsevier.

Llàcer Navarro, S., Nakayama, K., Idström, A., Evenäs, L., Ström, A., & Nypelö, T. (2021). The effect of sulfate half-ester groups on cellulose nanocrystal periodate oxidation. *Cellulose*, *28*(15), 9633–9644. http://dx.doi.org/10.1007/s10570-021-04115-y.

Maekawa, E., Kosaki, T., & Koshijima, T. (1986). Periodate oxidation of mercerized cellulose and regenerated cellulose. *Wood Research: Bulletin of the Wood Research Institute Kyoto University*, *73*, 44–49.

Morooka, T., Norimoto, M., & Yamada, T. (1989). Periodate oxidation of cellulose by homogeneous reaction. *Journal of Applied Polymer Science*, *38*(5), 849–858. http://dx.doi.org/10.1002/app.1989.070380508.

Münster, L., Vícha, J., Kloáč, J., Masař, M., Kucharczyk, P., & Kuřitka, I. (2017). Stability and aging of solubilized dialdehyde cellulose. *Cellulose*, *24*, 2753–2766.

Painter, T. J. (1988). Control of depolymerisation during the preparation of reduced dialdehyde cellulose. *Carbohydrate Research*, *179*, 259–268. http://dx.doi.org/10.1016/0008-6215(88)84123-5.

Palasingh, C., Nakayama, K., Abik, F., Mikkonen, K. S., Evenäs, L., Ström, A., & Nypelö, T. (2022). Modification of xylan via an oxidation–reduction reaction. *Carbohydrate Polymers*, *292*, Article 119660. http://dx.doi.org/10.1016/j.carbpol.2022.119660.

Palasingh, C., Ström, A., Amer, H., & Nypelö, T. (2021). Oxidized xylan additive for nanocellulose films – A swelling modifier. *International Journal of Biological Macromolecules*, *180*, 753–759. http://dx.doi.org/10.1016/j.ijbiomac.2021.03.062.

Pedersen, J. S. (1997). Analysis of small-angle scattering data from colloids and polymer solutions: modeling and least-squares fitting. *Advances in Colloid and Interface Science*, *70*, 171–210. http://dx.doi.org/10.1016/S0001-8686(97)00312-6.

Pedersen, J. S., & Schurtenberger, P. (2004). Scattering functions of semidilute solutions of polymers in a good solvent. *Journal of Polymer Science Part B: Polymer Physics*, *42*(17), 3081–3094.

Pellegrino, E., Al-Rudainy, B., Larsson, P. A., Fina, A., & Lo Re, G. (2025). Impact of water plasticization on dialcohol cellulose fibres melt processing-structure-properties relationship. *Carbohydrate Polymer Technologies and Applications*, *9*, Article 100642. http://dx.doi.org/10.1016/j.carpta.2024.100642.

Plazzotta, B., Diget, J. S., Zhu, K., Nyström, B., & Pedersen, J. S. (2016). Small-angle X-ray scattering as a useful supplementary technique to determine molecular masses of polyelectrolytes in solution. *Journal of Polymer Science Part B: Polymer Physics*, *54*(19), 1913–1917. http://dx.doi.org/10.1002/polb.24107.

Potthast, A., Kostic, M., Schiehser, S., Kosma, P., & Rosenau, T. (2007). Studies on oxidative modifications of cellulose in the periodate system: Molecular weight distribution and carbonyl group profiles. *Holzforschung*, *61*(6), 662–667. http://dx.doi.org/10.1515/HF.2007.099.

Potthast, A., Schiehser, S., Rosenau, T., & Kostic, M. (2009). Oxidative modifications of cellulose in the periodate system – Reduction and beta-elimination reactions 2nd ICC 2007, Tokyo, Japan, October 25–29, 2007. *Holzforschung*, *63*(1), 12–17. http://dx.doi.org/10.1515/HF.2009.108.

Prückler, M., Siebenhandl-Ehn, S., Apprich, S., Höltinger, S., Haas, C., Schmid, E., & Kneifel, W. (2014). Wheat bran-based biorefinery 1: Composition of wheat bran and strategies of functionalization. *LWT - Food Science and Technology*, *56*(2), 211–221. http://dx.doi.org/10.1016/j.lwt.2013.12.004.

Schooneveld-Bergmans, M., Beldman, G., & Voragen, A. (1999). Structural features of (Glucurono)arabinoxylans extracted from wheat bran by barium hydroxide. *Journal of Cereal Science*, *29*(1), 63–75. http://dx.doi.org/10.1006/jcrs.1998.0222.

Scott, J. E., & Thomas, D. P. (1976). Spectrofluorimetric detection and measurement of hydroxyl radicals in periodate solution. *Carbohydrate Research*, *52*(1), 214–218. http://dx.doi.org/10.1016/S0008-6215(00)85962-5.

Simon, J., Fliri, L., Sapkota, J., Ristolainen, M., Miller, S. A., Hummel, M., Rosenau, T., & Potthast, A. (2023). Reductive amination of dialdehyde cellulose: Access to renewable thermoplastics. *Biomacromolecules*, *24*(1), 166–177. http://dx.doi.org/10.1021/acs.biomac.2c01022.

Simon, J., Schlapp-Hackl, I., Sapkota, J., Ristolainen, M., Rosenau, T., & Potthast, A. (2024). Towards tailored dialdehyde cellulose derivatives: A strategy for tuning the glass transition temperature. *ChemSusChem*, *17*(5), Article e202300791. http://dx.doi.org/10.1002/cssc.202300791.

Veelaert, S., de Wit, D., Gotlieb, K., & Verhé, R. (1997). The gelation of dialdehyde starch. *Carbohydrate Polymers*, *32*(2), 131–139. http://dx.doi.org/10.1016/S0144-8617(96)00160-9.

Vold, I. M. N., Kristiansen, K. A., & Christensen, B. E. (2006). A study of the chain stiffness and extension of alginates, in vitro epimerized alginates, and periodate-oxidized alginates using size-exclusion chromatography combined with light scattering and viscosity detectors. *Biomacromolecules*, *7*(7), 2136–2146. http://dx.doi.org/10.1021/bm060099n.

Yao, H., Wang, Y., Yin, J., Nie, S., & Xie, M. (2021). Isolation, physicochemical properties, and structural characteristics of arabinoxylan from hull-less barley. *Molecules*, *26*(10), http://dx.doi.org/10.3390/molecules26103026.